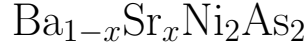


Giant nematic response of the incommensurate
charge density wave in the nickel-pnictide



Thomas Johnson^{1, 2}, Sangjun Lee³, Camille Bernal-Choban^{1, 2*},
Xuefei Guo^{1, 2}, Stella Sun^{1, 2}, John Collini⁴,
Christopher Eckberg⁴, Johnpierre Paglione^{4, 5},
Rafael M. Fernandes^{1, 6}, Eduardo Fradkin^{1, 6}, Peter Abbamonte^{1, 2*}

¹Department of Physics, The Grainger College of Engineering,
University of Illinois Urbana–Champaign, Urbana, 61801, IL, USA.

²Materials Research Laboratory, The Grainger College of Engineering,
University of Illinois Urbana–Champaign, Urbana, 61801, IL, USA.

³Samsung Institute of Advanced Technology, KOR.

⁴Maryland Quantum Materials Center, Department of Physics,
University of Maryland, College Park, 20742, MD, USA.

⁵Canadian Institute for Advanced Research, Toronto, Ontario M5G 1Z8,
Canada.

⁶Anthony J. Leggett Institute for Condensed Matter Theory, The
Grainger College of Engineering, University of Illinois
Urbana-Champaign, Urbana, 61801, IL, USA.

*Corresponding author(s). E-mail(s): cmcb@illinois.edu;
abbamonte@illinois.edu;

Abstract

Electron nematicity—the breaking of rotational symmetry while preserving translational symmetry—is the quantum analogue of classical nematic liquid crystals. First predicted in 1998, electronic nematicity has been established in a variety of materials, including two-dimensional electron gases (2DEGs) in magnetic

fields, copper-oxide superconductors, and Fe-based superconductors. A long-standing open question is what physical mechanisms drive electronic nematic order. In BaFe_2As_2 and highly underdoped $\text{YBa}_2\text{Cu}_3\text{O}_{6+y}$, strong evidence suggests that nematicity arises from vestigial spin-density-wave (SDW) order. However, evidence for nematicity associated with charge-density-wave (CDW) order has been less conclusive, particularly in systems near a superconducting state. Here, we present direct evidence for CDW-driven nematic fluctuations in the pnictide superconductor $\text{Ba}_{1-x}\text{Sr}_x\text{Ni}_2\text{As}_2$ (BSNA), a Ni-based homologue of Fe-based superconductors that exhibits CDW rather than SDW order. Previous elasto-resistance studies have shown that BSNA displays a large nematic susceptibility—linked to a six-fold enhancement of superconductivity—within a region of the phase diagram occupied by an incommensurate CDW. Using x-ray scattering under uniaxial strain, we demonstrate that even minimal strain levels ($\epsilon \sim 10^{-4}$) significantly break the fourfold symmetry of the CDW. Within a Ginzburg-Landau framework, we define a nematic susceptibility based on the asymmetric response of symmetry-related CDW superlattice reflections, showing strong agreement with elasto-resistivity measurements. Our study provides the first clear demonstration of a direct link between charge order and a nematic state, offering key insights into the intertwined superconducting phases of these materials.

Keywords: correlated materials, electronic nematicity, x-ray diffraction, uniaxial strain

Introduction

Electronic nematicity, the quantum counterpart of the classical liquid-crystalline order [1], has been reported in a variety of materials, including quantum Hall systems [2–6], copper-oxides [7–10] iron-based superconductors [11–14], correlated oxides [15], twisted bilayer graphene [16], and cold atoms in optical lattices [17]. Identifying the underlying mechanisms that drive electronic nematicity, however, is challenging. While elasto-resistivity [11] and Raman spectroscopy [18] measurements can disentangle whether electronic or lattice degrees of freedom drive the nematic instability, most of the relevant systems display ordering phenomena in different electronic degrees of freedom, such as spin, orbital, or charge [19], raising the question of whether such symmetry-breaking phenomena are integral for forming a nematic phase.

In iron pnictides [20], nematic order is best established and is generally understood to arise as a consequence of the nearby spin density wave order [19, 21, 22]. This phenomenon is usually explained by the concept of vestigial order, in which a composite order parameter condenses before the onset of the primary order. Vestigial order in this case emerges due to the proximity of nematic and stripe antiferromagnetic transition lines in the phase diagram [8, 23, 24]. Strong evidence for this mechanism is found in the observed scaling between the elastic shear modulus and the spin-lattice relaxation rate across different members of the 122 iron pnictide family [25–27], although many details of this process remain unsettled [28].

Electron nematic order may also occur at a quantum phase transition via a d -wave Pomeranchuk instability of a Fermi liquid [29], in which case it is continuously connected to a CDW transition [8, 23, 30]. Such an effect could occur, for example, near a CDW instability that breaks rotational symmetry by selecting one of two CDW wave vectors related by a 90° rotation [30].

The emergence of an electronic nematic order parameter associated with charge density wave (CDW) order, however, has not yet been established. While a charge-driven mechanism for nematicity may be relevant in the cuprates, direct evidence is still lacking. Recently, kagome metals have been proposed as potential hosts of CDW-driven nematicity, but experimental results so far have been contradictory [31–33].

Meanwhile, the $\text{Ba}_{1-x}\text{Sr}_x\text{Ni}_2\text{As}_2$ (BSNA) family of superconductors is a promising candidate for charge order-driven nematicity [34–39]. These materials serve as a non-magnetic analog of the 122 iron-pnictide superconductors [34, 40], and exhibit confirmed electronic nematicity [34, 35] and multiple CDWs [41]. The nematic phase in BSNA has also been linked to a sixfold enhancement of the superconducting transition temperature, suggesting an intertwining between nematicity and superconductivity [42].

Here, we present direct experimental evidence that electronic nematic fluctuations in BSNA are driven by charge density wave fluctuations. Using x-ray diffraction measurements on $\text{Ba}_{1-x}\text{Sr}_x\text{Ni}_2\text{As}_2$ with $x = 0.27$, we observe a giant anisotropic response of the symmetry-related incommensurate CDW superlattice reflections under small applied uniaxial strain. Defining a nematic order parameter based on this anisotropy, we compute the charge-nematic susceptibility and find excellent agreement with previous transport measurements of elasto-resistivity [34]. Furthermore, by fitting the x-ray-determined CDW anisotropy to a Ginzburg-Landau model, we reveal a strong anharmonic coupling between charge-nematic fluctuations and strain. Our study provides the first clear demonstration of a direct connection between charge order and a nematic state, with significant implications for understanding the intertwined superconducting state observed in these materials.

Results

X-ray diffraction experiments were performed on $\text{Ba}_{1-x}\text{Sr}_x\text{Ni}_2\text{As}_2$ (BSNA), $x = 0.27$, crystals grown by the self-flux method (Ref. [43]) and characterized in Ref. [41]. A piezoelectric strain device, identical to those employed in previous transport studies [13, 34], was used to apply uniaxial strain, ϵ , along the sample's tetragonal \mathbf{b} -axis, breaking C_4 rotational symmetry in the B_{1g} channel. At each applied strain, we collected cooling and heating measurements using a Xenocs GeniX^{3D} Mo $K\alpha$ ($\lambda = 0.7093\text{\AA}$) micro-spot x-ray source with a Mar345 image plate detector, with the sample and strain cell residing in a liquid helium cryostat with beryllium windows. Our strain value, ϵ , ranged from ~ 0 to 1.3×10^{-3} with an estimated error of 7×10^{-5} . Additional details of sample preparation and experimental setup are in the Methods section.

At a substitution of $x = 0.27$, BSNA hosts both a commensurate (C) and an incommensurate (I) charge density wave (CDW) [34, 41]. The I-CDW exists in the tetragonal

phase and exhibits fourfold rotational symmetry, with wave vectors $(0.28, 0, 0)_{\text{tet}}$ and $(0, 0.28, 0)_{\text{tet}}$ [41]. Notably, the I-CDW appears in the same region of the phase diagram where the nematic response observed in transport is most pronounced [34]. In contrast, the C-CDW, with wave vector $(1/3, 0, 0)_{\text{tri}}$, forms in the triclinic (low-temperature) phase, where rotational symmetry is explicitly broken, leading to a complex pattern of twin domains. Due to its relative simplicity and its connection to the nematic response observed in transport [34], this study focuses on the I-CDW. This coherent “2Q” state retains rotational symmetry, which can be broken by applying a symmetry-breaking strain field.

We measure the temperature dependence of the I-CDW peaks along the x and y reciprocal space directions under various applied strain values. Specifically, we use the CDW superlattice reflections $\mathbf{Q}_x = (-0.28, 3, -5)_{\text{tet}}$ and $\mathbf{Q}_y = (-1, -1.72, -5)_{\text{tet}}$, which correspond to the x and y components of the CDW in the $(0, 3, -5)$ and $(-1, -2, 5)$ Brillouin zones, respectively. These reflections were chosen for convenience, and since their wave vectors are related by a 90° rotation, their relative intensity provides a direct measure of the CDW anisotropy in the (x, y) plane.

Our main results, presented in Fig. 1, show the integrated intensities of these two CDW reflections as a function of temperature over the range $107 \text{ K} < T < 167 \text{ K}$ for several applied strain values. To account for differences in the CDW structure factors in different Brillouin zones, we normalize the intensities of both reflections to their values at $T = 135 \text{ K}$ and $\epsilon = 0$ (see Supplementary Information Fig. S3). No hysteresis was observed between heating and cooling cycles, so only cooling data are shown. (Warming data are included in the Supplementary Information.)

The I-CDW reflections emerge below $T_{\text{IC}} = 151 \text{ K}$, grow continuously with decreasing temperature, and abruptly disappear below the triclinic transition at $T_{\text{tri}} \sim 125 \text{ K}$ [41] (see Supplementary Information Fig. S2 for details on transition temperature determination). Applying uniaxial strain increases the integrated intensity of the

Q_x reflection while decreasing that of Q_y , demonstrating that even small values of applied strain break the fourfold rotational symmetry of the CDW.

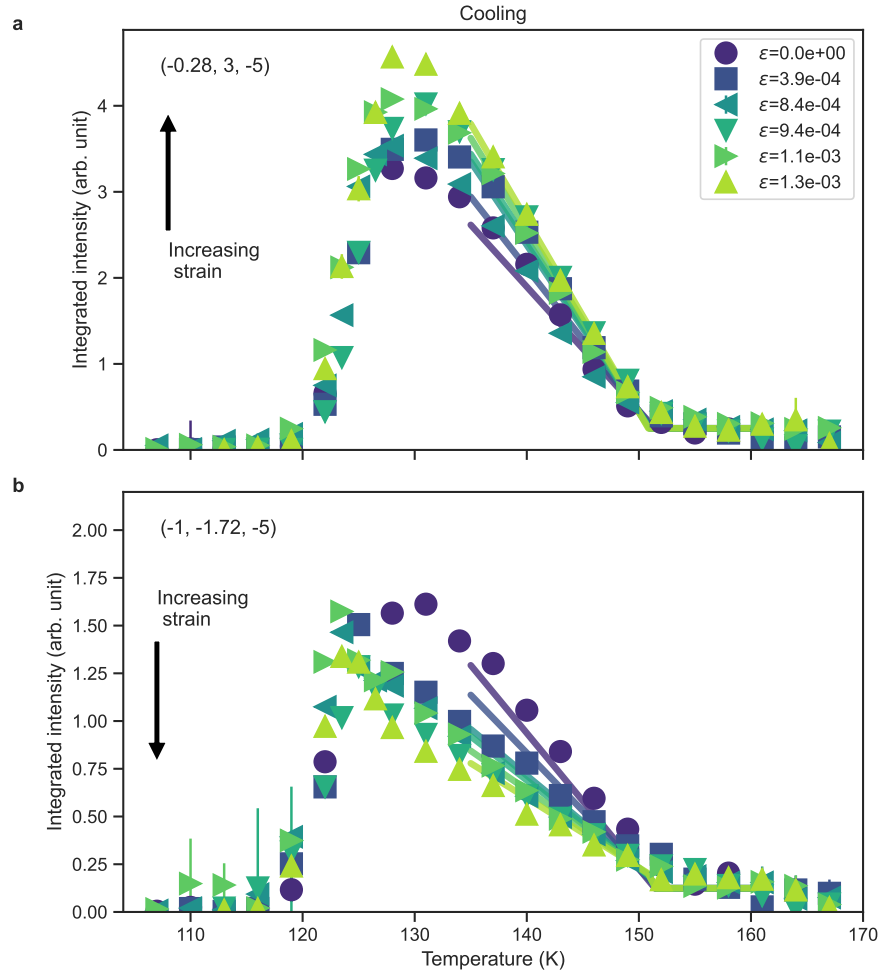


Fig. 1 Temperature dependence of two I-CDW satellites, related to one another by a 90° rotation, for various applied strain values. **a.** Integrated intensity of the $Q_x = (-0.28, 3, -5)_{tet}$ reflection, normalized to its value at $T = 135$ K at zero strain. **b.** Integrated intensity of the $Q_y = (-1, -1.72, -5)_{tet}$, also normalized to its value at $T = 135$ K at zero strain. Solid lines are fits to the data using the Landau model described in the text. Bars correspond to standard errors from least squares fits.

Following Ref. [23], we define a nematic order parameter based on the anisotropy of the I-CDW,

$$\Delta(\epsilon, T) = I_x(\epsilon, T) - I_y(\epsilon, T), \quad (1)$$

where I_x and I_y denote the integrated intensities of the \mathbf{Q}_x and \mathbf{Q}_y reflections, respectively, normalized to their values at $T = 135$ K. This anisotropy parameter, $\Delta(\epsilon, T)$, is odd under fourfold rotations around the c -axis and vanishes by definition when $\epsilon = 0$. It characterizes how the rotational symmetry of the I-CDW evolves with temperature and applied strain, analogous to the resistive anisotropy investigated in Ref. [34]. The full temperature and strain dependence of Δ is shown in Fig. 2. In the absence of strain, Δ remains zero except within a narrow temperature range below T_{tri} , where rotational symmetry is explicitly broken by the triclinic transition. However, upon applying strain of order $\epsilon \sim 10^{-4}$, we observe a nonzero Δ that emerges at T_{IC} and increases linearly with strain. This behavior becomes nonlinear below T_{tri} , where the I-CDW vanishes (see also Fig. S4). Notably, we do not observe a significant shift in the transition temperature T_{IC} across different strain values.

Discussion

As shown in Fig. 2, even small amounts of applied strain are sufficient to break the rotational symmetry of the I-CDW. Drawing an analogy to elastoresistivity studies that report a strong nematic response in BSNA [34], we define a CDW-nematic susceptibility as

$$\chi(T) = \frac{\partial \Delta(\epsilon, T)}{\partial \epsilon}, \quad (2)$$

which quantifies the sensitivity of the I-CDW to uniaxial strain. The temperature dependence of $\chi(T)$, obtained from a linear fit to the data in Fig. 2 (see Supplementary Information, Fig. S7), is shown in Fig. 3, alongside susceptibility data from elastoresistivity measurements reported in Ref. [34].

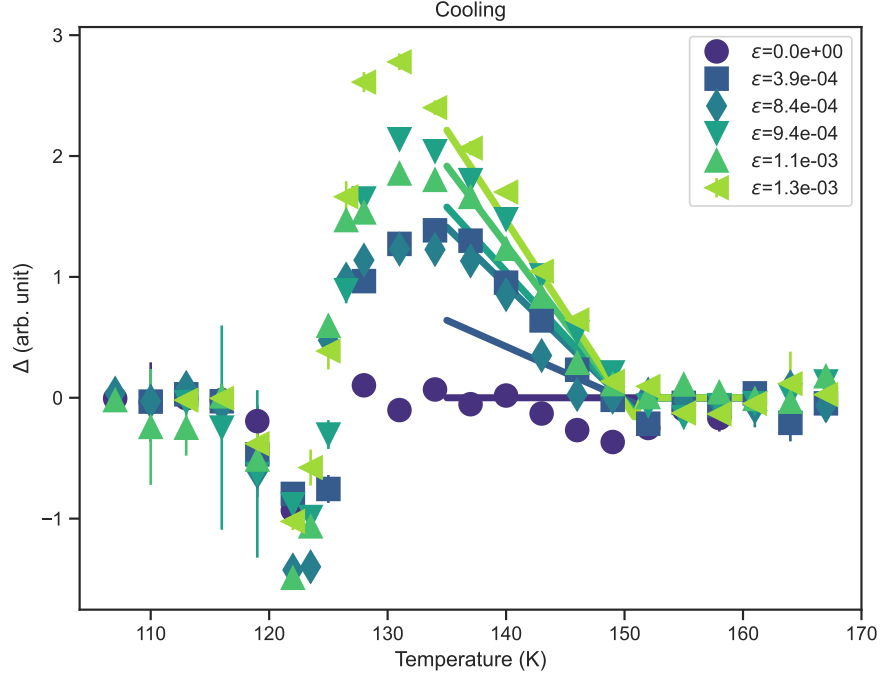


Fig. 2 Temperature dependence of the nematic order parameter, $\Delta = I_x - I_y$, which represents the rotational anisotropy of the I-CDW, for various applied strain values. The 90° rotational symmetry of the I-CDW is broken by even trace amounts ($\epsilon \sim 10^{-4}$) of strain. Solid lines correspond to the Landau fits described in the text. Bars represent standard errors from least squares fits.

The susceptibility curves obtained from x-ray and elastoresistivity studies show remarkable agreement (Fig. 3). Both datasets exhibit a similar profile: a nonzero response emerges around $\sim T_{IC}$, increases with decreasing temperature in the I-CDW regime following a Curie-Weiss trend, and vanishes at the triclinic transition. Additionally, our values of $\chi(T)$ for $x = 0.27$ fall almost exactly between those measured for $x = 0.2$ and $x = 0.4$ in elastoresistivity studies (Fig. 3). The strong correlation between x-ray and transport susceptibilities provides compelling evidence for a direct correspondence between the nematic order associated with I-CDW anisotropy and that observed in transport measurements. This observation also suggests that the nematic order originates from the I-CDW degrees of freedom.

We emphasize that the preservation of tetragonal symmetry in the I-CDW phase [41] is crucial for defining a nematic susceptibility from x-ray measurements. The translational symmetry-breaking potential imposed by the 2Q I-CDW order on the electronic degrees of freedom likely induces changes in the electronic spectrum, resulting in the nematic instability observed in transport studies [34]. This interpretation is supported by the fact that $\chi(T)$ remains essentially zero above T_{IC} .

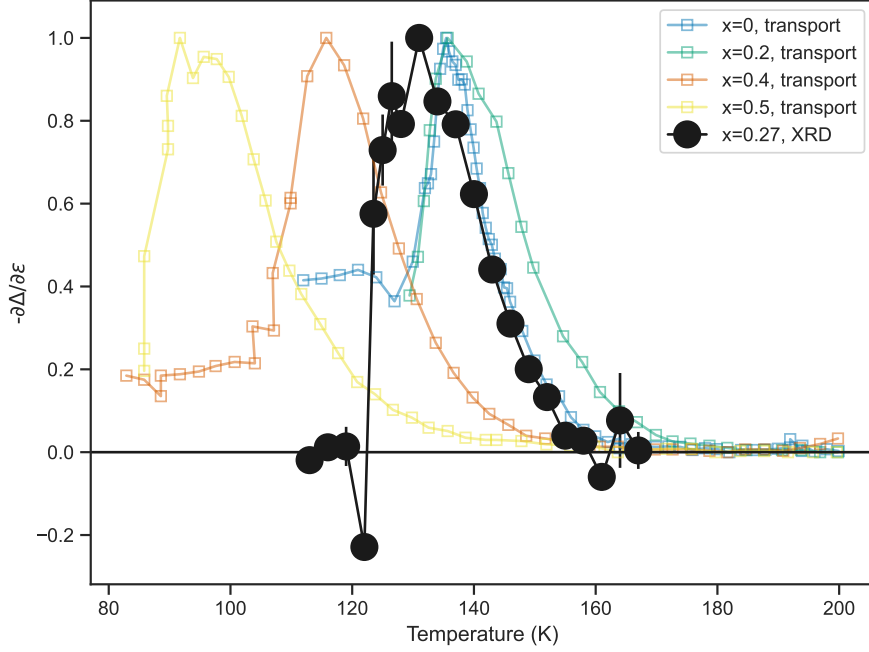


Fig. 3 Nematic susceptibility, $\chi(T)$ for BSNA with $x = 0.27$ (black circles) from our x-ray measurements. The data are plotted alongside nematic susceptibility data from the elastoresistivity measurements of Ref. [34] at similar substitutions (open squares). Remarkable consistency is seen between the two different techniques, suggesting the two effects have the same origin. Error bars for $x = 0.27$ correspond to standard errors from least squares fits.

Analyzing the symmetries within a simple Landau free energy framework provides significant insight into the coupling between the CDW and strain. To this end, we consider the Landau free energy for the I-CDW order parameter [24, 30],

$$F = F_0 + F_1 \quad (3)$$

where

$$F_0 = \frac{a}{2}(|\rho_x|^2 + |\rho_y|^2) + \frac{b}{4}(|\rho_x|^2 + |\rho_y|^2)^2 + \frac{c}{2}(|\rho_x|^2 - |\rho_y|^2)^2, \quad (4)$$

is the I-CDW free energy and

$$F_1 = -\lambda_\rho(|\rho_x|^2 - |\rho_y|^2)\epsilon, \quad (5)$$

describes the coupling between the I-CDW and strain. Here, ρ_x and ρ_y are complex amplitudes that characterize the I-CDW modulation along the x - and y - directions, i.e., the in-plane charge density is given by $\rho = \rho_0 + \rho_x e^{i\mathbf{Q}\cdot\hat{\mathbf{x}}} + \rho_y e^{i\mathbf{Q}\cdot\hat{\mathbf{y}}} + C.C$ with $|\rho_x|^2 \propto I_x$ and $|\rho_y|^2 \propto I_y$. The parameter $a(T) = a_0(T - T_{\text{IC}})$ denotes the proximity to the I-CDW transition temperature. The B_{1g} strain is given by $\epsilon_{xx} - \epsilon_{yy} = \epsilon_{xx}(1 + \nu) = \epsilon$, where ν represents the Poisson ratio for the piezo stack (see Methods). We assume that ν is constant over the temperature range investigated.

The CDW-strain coupling function, λ_ρ , can be expanded in powers of the (symmetric) CDW order parameter $|\rho|^2 \equiv |\rho_x|^2 + |\rho_y|^2$:

$$\lambda_\rho = \lambda + \lambda'|\rho|^2 + \mathcal{O}(|\rho|^4). \quad (6)$$

In most approaches, only the leading-order (harmonic) term is retained [19]. The primary effect of this term, λ , is to split the transition temperatures of the x - and y -modulated CDWs. However, the data in Fig. 1 show no such splitting, suggesting the need to include the higher-order coupling term, λ' . This term introduces anharmonic coupling, as the lattice distortion ϵ induced by unequal intensities at the two I-CDW wave vectors scales with the intensity squared, $|\rho|^4$, rather than linearly with $|\rho|^2$. Interestingly, a related anharmonic term has been proposed to explain the nature of the coupled nematic and magnetic transitions in the related iron-based compound BaFe_2As_2 [44].

Incorporating this additional coupling term, our total free energy (Eq. 3) successfully captures all features of the data for $T > 135$ K, above the triclinic transition. We overlay these free energy fits as solid lines in Fig. 1. First, we find that $c > 0$, consistent with the preservation of tetragonal symmetry in the I-CDW phase. Second, we determine that λ and λ' have opposite signs and similar magnitudes, with $\lambda = 39(3)$ and $\lambda' = -82(1)$. This result shows that anharmonic effects are essential to fully describe the influence of strain on the CDW degrees of freedom in BSNA.

Beyond establishing the role of anharmonic CDW-strain effects in BSNA, our analysis provides insights into the mechanism underlying the anisotropic resistivity associated with nematicity. Previously, the strong temperature dependence of the elastoresistance inside the I-CDW phase was attributed to an electronic contribution to the nematic order parameter [34]. Here, we showed that although the I-CDW phase does not break tetragonal symmetry, it hosts a sizable nematic susceptibility. Interestingly, this is also the case of the double-Q spin-density wave observed in the doped iron-pnictide compound $\text{CaKFe}_4\text{As}_4$ [45]. Moreover, similar to the spin degree of freedom in their iron-based counterparts, the charge degree of freedom in BSNA couples to strain through a bilinear term involving the antisymmetric component of charge density fluctuations, $(|\rho_x|^2 - |\rho_y|^2)$. A key difference, however, is that the nematicity in BSNA also depends on the symmetric combination, $(|\rho|^2)$. This additional dependence means that, unlike the iron-based spin-driven nematic systems, the overall and relative magnitudes of the density fluctuations contribute significantly to the nematicity of $\text{Ba}_{1-x}\text{Sr}_x\text{Ni}_2\text{As}_2$.

Since the nematic susceptibility only appears in the I-CDW regime, the resistivity anisotropy likely arises from the strain-induced difference in the two CDW ρ_x and ρ_y order parameters, implying a charge-driven nematicity. We postulate that this difference drives an anisotropic reconstruction of the Fermi surface, causing inequivalent averaged Fermi velocities along the x and y directions. The resulting Drude

weight anisotropy manifests as an anisotropy in the DC resistivity. The similarity between the temperature dependence of the I-CDW nematic susceptibility $\partial\Delta/\partial\epsilon$ and elasto-resistivity measurements provides further evidence for this scenario.

It is interesting to note that nematic fluctuations in BSNA have been associated with the sharp enhancement of the superconducting transition temperature observed upon substitution [34]. Our results demonstrate a significant anharmonic coupling between charge fluctuations and electronic nematicity. This raises the intriguing question of whether this anharmonic coupling contributes to the enhancement of T_c .

Methods

Our $\text{Ba}_{1-x}\text{Sr}_x\text{Ni}_2\text{As}_2$ (BSNA) $x = 0.27$ crystals were grown using the self-flux method described in Ref. [43] and characterized in Ref. [41]. We applied uniaxial strain using the commercial piezoelectric stack shown in Fig. 4. Before mounting the sample, it was polished to a $41\ \mu\text{m}$ thickness to ensure uniform applied strain. A thin layer of epoxy held the sample atop the piezo stack for measurements.

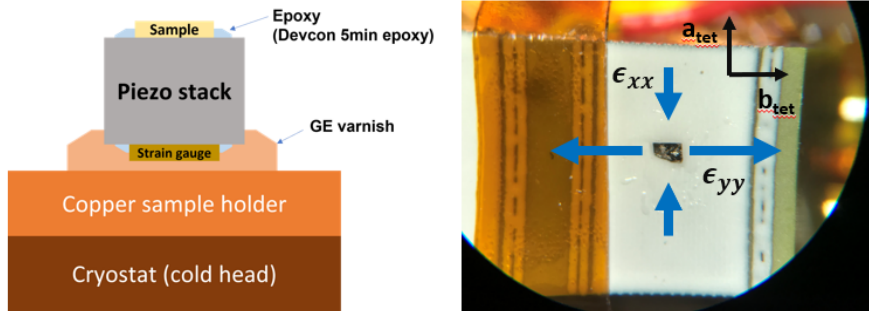


Fig. 4 Schematic of **a.** the piezoelectric stack (side view) used for applying uniaxial strain and **b.** directions of applied strain overlaid on the sample (top view). Tensile strain is directed along the tetragonal **b**-axis, resulting in a corresponding compressive strain along the **a**-axis due to Poisson's ratio.

Upon applying voltage, the piezo stack introduces a uniaxial (tensile) strain along the sample's tetragonal **b**-axis with a corresponding (compressive) strain directed along the tetragonal **a**-axis as dictated by Poisson's ratio. The amount of strain

applied was measured using a gauge mounted to the underside of the piezo stack with Crystalbond.

All x-ray diffraction measurements were performed using a Xenocs GeniX^{3D} Mo K α ($\lambda = 0.7093\text{\AA}$) micro-spot x-ray source with a Mar345 plate detector and liquid helium cryostat. Our strain setup was mounted on the cryostat and enclosed in a Be dome with wide angular access. We collected cooling and heating measurements at varying strains of up to 1.3×10^{-3} . The estimated error of applied strain, primarily due to thermal contraction, was 7×10^{-5} . Because nematicity couples linearly to small strains with the same symmetry [13], this setup probes rotational symmetry breaking in the B_{1g} channel, where a Curie-Weiss divergence of the nematic susceptibility was observed [34].

Supplementary information. Supplementary information containing diffraction peaks and additional details on determining transition temperatures and data fitting is available at [URL].

Acknowledgements. This work was primarily supported by the Center for Quantum Sensing and Quantum Materials, an Energy Frontier Research Center funded by the U.S. Department of Energy (DOE), Office of Science, Basic Energy Sciences (BES), under Award No. DE-SC0021238. Growth of BSNA crystals was supported by the AFOSR Grant No. FA9550-14-10332 and the National Science Foundation Grants No. DMR1905891 and No. DMR2225920, as well as the Maryland Quantum Materials Center and the Maryland Nanocenter and its FabLab. P.A. and J.P.P. gratefully acknowledge additional support from the EPiQS program of the Gordon and Betty Moore Foundation, Grants No. GBMF9452 and GBMF9071, respectively.

Declarations

Competing Interests

The authors declare no conflicts of interest.

Data Availability

All data is available at [URL].

Materials Availability

Code Availability

Not applicable.

Author Contribution

S. L., P. A., and J. P. conceptualized the hypothesis. Samples were grown by J.C. and C. E, and S. L., S.S., and P. A. designed the strain experiments. T. J. and S. L. took the x-ray diffraction measurements. T.J. performed the fits and subsequent analysis. X.G. wrote the x-ray diffraction analysis code. R.M.F. and E.F. developed the theoretical model. C. B-C., T.J., R.M.F., and P.A. wrote the manuscript.

References

- [1] Kivelson, S. A., Fradkin, E. & Emery, V. J. Electronic liquid-crystal phases of a doped mott insulator. *Nature* **393**, 550–553 (1998). URL <https://doi.org/10.1038/31177>.
- [2] Lilly, M. P., Cooper, K. B., Eisenstein, J. P., Pfeiffer, L. N. & West, K. W. Evidence for an anisotropic state of two-dimensional electrons in high Landau

- levels. Phys. Rev. Lett. **82**, 394–397 (1999). URL <https://link.aps.org/doi/10.1103/PhysRevLett.82.394>.
- [3] Pan, W. et al. Strongly anisotropic electronic transport at Landau level filling factor $\nu = 9/2$ and $\nu = 5/2$ under a tilted magnetic field. Physical Review Letters **83**, 820–823 (1999). URL <https://link.aps.org/doi/10.1103/PhysRevLett.83.820>.
- [4] Fradkin, E., Kivelson, S. A., Lawler, M. J., Eisenstein, J. P. & Mackenzie, A. P. Nematic Fermi Fluids in Condensed Matter Physics. Annual Review of Condensed Matter Physics **1**, 153–178 (2010). URL <https://doi.org/10.1146/annurev-conmatphys-070909-103925>.
- [5] Samkharadze, N. et al. Observation of a transition from a topologically ordered to a spontaneously broken symmetry phase. Nature Physics **12**, 191–195 (2016). URL <https://doi.org/10.1038/nphys3523>.
- [6] Qian, Q., Nakamura, J., Fallahi, S., Gardner, G. C. & Manfra, M. J. Possible nematic to smectic phase transition in a two-dimensional electron gas at half-filling. Nature Communications **8**, 1536 (2017). URL <https://doi.org/10.1038/s41467-017-01810-y>.
- [7] Hinkov, V. et al. Electronic liquid crystal state in the high-temperature superconductor $\text{YBa}_2\text{Cu}_3\text{O}_{6.45}$. Science **319**, 597–600 (2008). URL <https://www.science.org/doi/abs/10.1126/science.1152309>.
- [8] Fradkin, E., Kivelson, S. A. & Tranquada, J. M. Colloquium: Theory of intertwined orders in high temperature superconductors. Rev. Mod. Phys. **87**, 457–482 (2015). URL <https://link.aps.org/doi/10.1103/RevModPhys.87.457>.
- [9] Nakata, S. et al. Nematicity in a cuprate superconductor revealed by angle-resolved photoemission spectroscopy under uniaxial strain.

- npj Quantum Materials **6**, 1–6 (2021). URL <https://www.nature.com/articles/s41535-021-00390-x>.
- [10] Auvray, N. et al. Nematic fluctuations in the cuprate superconductor $\text{Bi}_2\text{Sr}_2\text{CaCu}_2\text{O}_{8+\delta}$. Nature Communications **10**, 5209 (2019). URL <https://www.nature.com/articles/s41467-019-12940-w>.
- [11] Chu, J.-H., Kuo, H.-H., Analytis, J. G. & Fisher, I. R. Divergent nematic susceptibility in an iron arsenide superconductor. Science **337**, 710–712 (2012).
- [12] Yi, M. et al. Symmetry-breaking orbital anisotropy observed for detwinned $\text{Ba}(\text{Fe}_{1-x}\text{Co}_x)_2\text{As}_2$ above the spin density wave transition. Proceedings of the National Academy of Sciences **108**, 6878–6883 (2011).
- [13] Kuo, H.-H., Chu, J.-H., Palmstrom, J. C., Kivelson, S. A. & Fisher, I. R. Ubiquitous signatures of nematic quantum criticality in optimally doped Fe-based superconductors. Science **352**, 958–962 (2016). URL <https://www.science.org/doi/10.1126/science.aab0103>.
- [14] Worasaran, T. et al. Nematic quantum criticality in an Fe-based superconductor revealed by strain-tuning. Science **372**, 973–977 (2021).
- [15] Borzi, R. A. et al. Formation of a nematic fluid at high fields in $\text{Sr}_3\text{Ru}_2\text{O}_7$. Science **315**, 214–217 (2007). URL <https://www.science.org/doi/10.1126/science.1134796>.
- [16] Cao, Y. et al. Nematicity and competing orders in superconducting magic-angle graphene. science **372**, 264–271 (2021).
- [17] Jin, S. et al. Evidence of Potts-nematic superfluidity in a hexagonal sp^2 optical lattice. Physical Review Letters **126**, 035301 (2021). URL <https://link.aps.org/>

[doi/10.1103/PhysRevLett.126.035301](https://doi.org/10.1103/PhysRevLett.126.035301).

- [18] Gallais, Y. & Paul, I. Charge nematicity and electronic raman scattering in iron-based superconductors. Comptes Rendus Physique **17**, 113–139 (2016).
- [19] Fernandes, R. M., Chubukov, A. V. & Schmalian, J. What drives nematic order in iron-based superconductors? Nature Physics **10**, 97–104 (2014). URL <https://www.nature.com/articles/nphys2877>.
- [20] Fernandes, R. M. et al. Iron pnictides and chalcogenides: a new paradigm for superconductivity. Nature **601**, 35–44 (2022).
- [21] Fang, C., Yao, H., Tsai, W.-F., Hu, J. & Kivelson, S. A. Theory of electron nematic order in LaFeAsO. Phys. Rev. B **77**, 224509 (2008). URL <https://link.aps.org/doi/10.1103/PhysRevB.77.224509>.
- [22] Xu, C., Müller, M. & Sachdev, S. Ising and spin orders in the iron-based superconductors. Physical Review B **78**, 020501 (2008). URL <https://link.aps.org/doi/10.1103/PhysRevB.78.020501>.
- [23] Nie, L., Tarjus, G. & Kivelson, S. A. Quenched disorder and vestigial nematicity in the pseudogap regime of the cuprates. Proceedings of the National Academy of Sciences **111**, 7980–7985 (2014). URL <https://pnas.org/doi/full/10.1073/pnas.1406019111>.
- [24] Fernandes, R. M., Orth, P. P. & Schmalian, J. Intertwined vestigial order in quantum materials: Nematicity and beyond. Annual Review of Condensed Matter Physics **10**, 133–154 (2019). URL <https://www.annualreviews.org/doi/10.1146/annurev-conmatphys-031218-013200>.

- [25] Fernandes, R. M., Böhrer, A. E., Meingast, C. & Schmalian, J. Scaling between magnetic and lattice fluctuations in iron pnictide superconductors. Physical Review Letters **111**, 137001 (2013). URL <https://link.aps.org/doi/10.1103/PhysRevLett.111.137001>.
- [26] Böhrer, A. E. et al. Nematic susceptibility of hole-doped and electron-doped BaFe₂As₂ iron-based superconductors from shear modulus measurements. Phys. Rev. Lett. **112**, 047001 (2014). URL <https://link.aps.org/doi/10.1103/PhysRevLett.112.047001>.
- [27] Lu, X. et al. Nematic spin correlations in the tetragonal state of uniaxial-strained BaFe_{2-x}Ni_xAs₂. Science **345**, 657–660 (2014). URL <https://www.science.org/doi/full/10.1126/science.1251853>.
- [28] Böhrer, A. E., Chu, J.-H., Lederer, S. & Yi, M. Nematicity and nematic fluctuations in iron-based superconductors. Nature Physics **18**, 1412–1419 (2022).
- [29] Oganesyan, V., Kivelson, S. A. & Fradkin, E. Quantum theory of a nematic Fermi fluid. Physical Review B **64**, 195109 (2001). URL <https://link.aps.org/doi/10.1103/PhysRevB.64.195109>.
- [30] Nie, L., Maharaj, A. V., Fradkin, E. & Kivelson, S. A. Vestigial nematicity from spin and/or charge order in the cuprates. Physical Review B **96**, 085142 (2017). URL <https://link.aps.org/doi/10.1103/PhysRevB.96.085142>.
- [31] Nie, L. et al. Charge-density-wave-driven electronic nematicity in a kagome superconductor. Nature **604**, 59–64 (2022). URL <https://www.nature.com/articles/s41586-022-04493-8>.
- [32] Grandi, F., Consiglio, A., Sentef, M. A., Thomale, R. & Kennes, D. M. Theory of nematic charge orders in kagome metals. Physical Review B **107**, 155131 (2023).

URL <https://link.aps.org/doi/10.1103/PhysRevB.107.155131>.

- [33] Asaba, T. et al. Evidence for an odd-parity nematic phase above the charge-density-wave transition in a kagome metal. Nature Physics **20**, 40–46 (2024). URL <https://www.nature.com/articles/s41567-023-02272-4>.
- [34] Eckberg, C. et al. Sixfold enhancement of superconductivity in a tunable electronic nematic system. Nature Physics **16**, 346–350 (2020). URL <https://www.nature.com/articles/s41567-019-0736-9>.
- [35] Yao, Y. et al. An electronic nematic liquid in BaNi_2As_2 . Nature Communications **13**, 4535 (2022).
- [36] Souliou, S. M. et al. Soft-phonon and charge-density-wave formation in nematic BaNi_2As_2 . Phys. Rev. Lett. **129**, 247602 (2022). URL <https://link.aps.org/doi/10.1103/PhysRevLett.129.247602>.
- [37] Song, Y. et al. Phonon softening and slowing-down of charge density wave fluctuations in BaNi_2As_2 . Phys. Rev. B **107**, L041113 (2023). URL <https://link.aps.org/doi/10.1103/PhysRevB.107.L041113>.
- [38] Frachet, M. et al. Elastoresistivity in the incommensurate charge density wave phase of $\text{BaNi}_2(\text{As}_{1-x}\text{P}_x)_2$. npj Quantum Materials **7**, 115 (2022).
- [39] Chen, Y. et al. Charge density fluctuations with enhanced superconductivity at the proposed nematic quantum critical point (2024). URL <http://arxiv.org/abs/2410.03956>.
- [40] Narayan, D. M. et al. Potential lifshitz transition at optimal substitution in nematic pnictide $\text{Ba}_{1-x}\text{Sr}_x\text{Ni}_2\text{As}_2$. Science Advances **9** (2023). URL <https://www.science.org/doi/abs/10.1126/sciadv.adi4966>.

- [41] Lee, S. et al. Multiple charge density waves and superconductivity nucleation at antiphase domain walls in the nematic pnictide $\text{Ba}_{1-x}\text{Sr}_x\text{Ni}_2\text{As}_2$. Physical Review Letters **127**, 027602 (2021). URL <https://link.aps.org/doi/10.1103/PhysRevLett.127.027602>.
- [42] Lederer, S., Berg, E. & Kim, E.-A. Tests of nematic-mediated superconductivity applied to $\text{Ba}_{1-x}\text{Sr}_x\text{Ni}_2\text{As}_2$. Phys. Rev. Res. **2**, 023122 (2020). URL <https://link.aps.org/doi/10.1103/PhysRevResearch.2.023122>.
- [43] Sefat, A. S. et al. Structure and anisotropic properties of $\text{BaFe}_{2-x}\text{Ni}_x\text{As}_2$ ($x=0, 1, \text{ and } 2$) single crystals. Physical Review B **79**, 094508 (2009). URL <https://link.aps.org/doi/10.1103/PhysRevB.79.094508>.
- [44] Kim, M. G. et al. Character of the structural and magnetic phase transitions in the parent and electron-doped BaFe_2As_2 compounds. Physical Review B **83**, 134522 (2011). URL <https://link.aps.org/doi/10.1103/PhysRevB.83.134522>.
- [45] Böhmer, A. E. et al. Evolution of nematic fluctuations in $\text{CaK}(\text{Fe}_{1-x}\text{Ni}_x)_4\text{As}_4$ with spin-vortex crystal magnetic order (2020). URL <http://arxiv.org/abs/2011.13207>.